

# IGA Based Bi-Layer Fiber Angle Optimization Method for Variable Stiffness Composites

Chao Mei, Qifu Wang\*, Chen Yu and Zhaohui Xia

School of Mechanical Science and Engineering, Huazhong University of Science and Technology, Wuhan, 430074, China

\*Corresponding Author: Qifu Wang. Email: wangqf@hust.edu.cn

Received: 30 January 2020; Accepted: 20 March 2020

**Abstract:** This paper presents a topology optimization method for variable stiffness composite panels with varying fiber orientation and curvilinear fiber path. Non-uniform rational B-Splines (NURBS) based Isogeometric analysis (IGA) is utilized for the numerical computation of the general minimum compliance problem. The sensitivity analysis of the structure compliance function for the density and bi-layer orientation is conducted. The bi-layer fiber paths in the design domain are generated using streamline method and updated by divided pieces reselection method after the optimization process. Several common examples are tested to demonstrate the effectiveness of the method. The results show that the proposed method can generate more manufacturable fiber paths than some typical topology optimization methods.

**Keywords:** Isogeometric analysis; fiber angle optimization; variable stiffness composites

## 1 Introduction

Fiber reinforced composite materials have been widely applied in the automotive and aerospace industries because of their high strength-to-weight ratios [1–5]. With the emergence of advanced manufacturing technology et al Automated Fiber Placement (AFP) [6–8], variable-stiffness composite panels with curvilinear fiber path can be manufactured. According to the previous studies [4,7], such variable-stiffness composites (VSC) are more promising for lightweight structure design and optimization compared with the traditional fiber-reinforced composites. Since the mechanical properties of VSC strongly depend on the fiber orientations, a large amount of efforts have been made to optimize the fiber orientations, as well as the material distributions using a variety of numerical strategies [5,9–11].

Topology optimization [12] is one of the most widely used structural optimization techniques for both isotropic material structures [13–18] and composite structures [10,19,20]. In recent years, efficient topology optimization methods have been developed, such as data-driven optimization method [21], high-efficiency isogeometric topology optimization method [18,22,23] and feature-driven optimization method (FDO) [14,24,25].

For optimization of anisotropic composites, Stegmann et al. [20] used a solid isotropic material penalization (SIMP) approach to solve the anisotropic multi-layer laminates topology optimization problem. To exclusively deal with fiber orientations, discrete material optimization (DMO) was proposed



This work is licensed under a Creative Commons Attribution 4.0 International License, which permits unrestricted use, distribution, and reproduction in any medium, provided the original work is properly cited.

[19,20]. The manufacturing constraint problems based on the DMO have been studied [26]. The element angles are set as design variables and they are constantly updated to several specific constant values such as  $(0^\circ, \pm 45^\circ, 90^\circ)$  in the optimization process. Similar methods such as the shape functions with penalization (SFP) [27,28], and the bi-value coding parameterization method (BCP) [29,30] were developed. The element angles in these two methods are constantly updated by attaching to the shape functions and logic bi-values respectively. Zhou et al. [31] proposed a multi-component topology and material orientation optimization method (MTO-C) to optimize the densities and fiber angles for the composite materials. The multi-components were employed to represent a set of materials with different fiber orientations. In these methods, the fiber angles are set as several candidate values in the design patches. The optimization problems are treated as multi-material topology optimization problems. The free material optimization (FMO) method takes the material performance parameters as the variables instead of element angles. Both the distribution of material and the material itself can be freely varied in the FMO method [32,33]. As most of the fiber paths in variable-stiffness composites are curvilinear and the fiber angles varied in the design domain, the most significant material parameters are the fiber angles. The continuous fiber angle optimization method (CFAO) uses the continuous element fiber angles as the design variables. As studied in the literatures [8,10,34], the CFAO method are effective to optimize the fiber angles, but the continuous spatial variation of fiber angle may lead to local minima problems. Different strategies such as Shepard interpolation [34], iso-parametric projection method [10], Poisson's equation for material orientation optimization [35], and the normal distribution fiber optimization with fiber continuity (NDFO-C) method [8] are employed to improve the manufacturability of the fibers.

The optimization techniques mentioned in the previous references generated and optimized the fiber path based on the local fiber angles [6,10]. These fiber path generation methods are called indirect parameterization techniques [8]. The disadvantage of these indirect methods is that additional treatment considering manufacturability constraints is necessary in case of poor manufacturability, such as discontinuous, and large curvature of the fiber paths. There is another method to generate and optimize the fiber path called the "top-down" method. The fiber paths are firstly predefined by various parameters and then the local element angles are calculated according to the tangent angle of the fiber paths. The paths are directly optimized using the fiber path parameters as design variables [4,7,36–40]. Variety of shape description functions, such as linear variation function [4], flow field function [7,36–40] and cubic polynomial function [7,36–38] are employed to describe the fiber paths. These methods are more convenient to obtain fiber geometric information and manufacturability constraints, such as fiber path curvatures, gaps and overlaps. However, the geometric complexity of the fiber paths is limited [8,39].

As the geometric complexity may lead to numerical computation accuracy problems in the general structure response analysis process, a new numerical computation method called isogeometric analysis (IGA) is used to improve the accuracy and effectiveness [7,36–40]. The IGA [41] is a novel efficient numerical method in modern computational mechanics [42]. The application of the IGA in shape and topology optimization problems for variable stiffness composite shells are widely studied [7,36–38]. This method shows advantages over traditional FEA methods in variable-stiffness fiber angle optimization problems. It is found that the IGA is extremely suitable for shape and topology optimization of complex shells and the VSC because of the accurate geometric representation and high-order continuity. Since the element fiber angles differ in the design domain, high continuous basis functions are needed to ensure the continuity of mechanical property along with the fiber path directions.

The concept of the IGA is firstly proposed by Hughes and his co-workers in 2005 [42]. Since then the IGA received wide attention from researchers and developed rapidly in a variety of domains [43–46]. The IGA directly uses the basis functions of a computer-aided design (CAD) model as the shape functions of the computer-aided engineering (CAE) analysis model. The analysis element models exactly represent the

geometry of the structures. Generally, the IGA models are based on NURBS [16,18,23], which is the most thoroughly developed and most widely used CAD technology. In addition, high-order elements are used with  $k$ -refinement strategies, which are very efficient and robust for solving physical problems [41,42]. The IGA is more accurate than other CAE methods, such as finite element method (FEM), boundary element method (BEM) and Meshless methods, especially for handling the model with complex boundaries [15,17,22,23]. Due to the high accuracy and high continuity, the IGA is widely used in shape optimization [47,48] and topology optimization [18,49,50] problems to overcome the drawbacks of the traditional FEM. The applications of the IGA in structural optimization are comprehensively reviewed in [18].

Most of former references considered single layer fiber angle optimization problems [29–35]. However, most of the straight fiber and variable-stiffness fiber-reinforced composites are manufactured by multiple layers [51,52]. Multi-layered fiber angle optimization problems are considered in some of the former literatures [7,36–40]. The two-layered variable-stiffness composites optimization problems and some stiffen structure optimization problems also play an important part in composite structure design and optimization [39,51–53].

In this paper, a bi-layer continuous fiber angle optimization (Bi-CFAO) method based on the IGA is proposed to optimize the element densities and two-layered variable-stiffness composite fiber angles. The fiber paths are generated using streamline functions. The partition reselection procedure is used to recombine the local discontinuous regions and to generate the continuous fiber paths. Continuous fiber paths are generated without local small curvatures, thus retaining the optimal result information of the local element fiber angles to the maximum extent. Several numerical examples are presented to illustrate the proposed method.

The organization of this paper is as follows. Section 2 briefly introduces the fundamentals of the IGA framework and the basic theory of SIMP based Bi-CFAO method. Section 3 describes the proposed IGA based Bi-CFAO method. And the numerical implementations are introduced. In Section 4, the fiber path generation process and the density and angle optimization procedures are presented. Thereafter benchmark examples and discussions are presented in Section 5 to demonstrate the efficiency and stability of the proposed method. Finally, conclusion and future research are summarized in Section 6.

## 2 Basic Theory

### 2.1 Summary of NURBS for IGA

In the IGA [18,49,50], non-uniform rational B-splines (NURBS), constructed from B-splines, are commonly used for the numerical discretization [54–57]. A knot vector  $\mathbf{II}$ , which consists of  $n$  spline basis functions, is a sequence of non-decreasing real numbers representing parametric coordinates of a curve:

$$\mathbf{II} = \{\eta_1, \eta_2, \dots, \eta_{n+p+1}\} \quad (1)$$

where  $p$  is the order of the B-spline. The interval  $[\eta_i, \eta_{i+p+1}]$  is called a patch, and the knot interval  $[\eta_i, \eta_{i+1})$  is called a span. Given a knot vector, the B-spline basis functions are recursively defined following the Cox-de Boor formula [58]:

For zero-order ( $p = 0$ ),

$$B_{i,p}(\eta) = \begin{cases} 1 & \text{if } \eta_i \leq \eta < \eta_{i+1} \\ 0 & \text{otherwise} \end{cases} \quad (2)$$

And non-zero order ( $p > 0$ )

$$B_{i,p}(\eta) = \frac{\eta - \eta_i}{\eta_{i+p} - \eta_i} B_{i,p-1}(\eta) + \frac{\eta_{i+p+1} - \eta}{\eta_{i+p+1} - \eta_{i+1}} B_{i+1,p-1}(\eta) \quad (3)$$

It is observed that the B-spline basis functions constitute a partition of unity.

$$\sum_{i=1}^n B_{i,p}(\eta) = 1 \quad (4)$$

Two-dimensional B-spline basis functions are constructed as tensor products,

$$B_{i,p}^{j,q}(\eta, \xi) = B_{i,p}(\eta) B_{j,q}(\xi) \quad (5)$$

where  $B_{i,p}(\eta)$  and  $B_{j,q}(\xi)$  are univariate B-spline basis functions of order  $p$  and  $q$ , corresponding to knot vectors  $\mathbf{\Pi} = \{\eta_1, \eta_2, \dots, \eta_{n+p+1}\}$  and  $\mathbf{\Psi} = \{\xi_1, \xi_2, \dots, \xi_{m+q+1}\}$ .

A bivariate B-spline surface is obtained as the tensor product of two B-spline curves

$$S(\eta, \xi) = \sum_{i=1}^n \sum_{j=1}^m B_{i,p}^{j,q}(\eta, \xi) P_{i,j} \quad (6)$$

where  $P_{i,j}$  are the control points. The patch for the surface is now the domain  $[\eta_1, \eta_{n+p+1}] \times [\xi_1, \xi_{m+q+1}]$ .

NURBS basis functions are obtained from B-splines by assigning a positive weight  $\omega_i$  to each basis function

$$N_{i,p}(\eta) = \frac{B_{i,p}(\eta) \omega_i}{\sum_{j=1}^n B_{j,p}(\eta) \omega_j} \quad (7)$$

The basis functions for two-dimensional NURBS are constructed as

$$N_{i,p}^{j,q}(\eta, \xi) = \frac{B_{i,p}(\eta) B_{j,q}(\xi) \omega_{i,j}}{\sum_{k=1}^n \sum_{l=1}^m B_{k,p}(\eta) B_{l,q}(\xi) \omega_{k,l}} \quad (8)$$

where  $\omega_{i,j}$  is the weight value of the control point  $P_{i,j}$  in the NURBS surface. And  $\omega_{i,j}$  is corresponding to the tensor product  $B_{i,p}(\eta) B_{j,q}(\xi)$  and the control point  $P_{i,j}$ . Note that if the weights of rational basis functions are all equal, then NURBS becomes B-splines. And note that for the circle, cylinder, cone, and sphere the weight values are not equal. They should be determined by the shape of the curves, surfaces and the control points. More details are referred to [16,37,56].

In IGA, these basis functions are used for both shape representation and physical field approximation. A NURBS surface of order  $p$  in  $\eta$  direction and order  $q$  in direction  $\xi$  is a bivariate piecewise rational function of the form

$$S(\eta, \xi) = \sum_{i=1}^n \sum_{j=1}^m N_{i,p}^{j,q}(\eta, \xi) P_{i,j} \quad (9)$$

where  $P_{i,j}$  are the control points in this paper. It should be noted that  $P_{i,j}$  can refer to either the control points or a specific physical quantity that is associated with [22,41,42].

## 2.2 Basic Theory of SIMP Based Bi-CFAO Method

In general, the SIMP approach takes element density as design variable and then analyzes the effectiveness of the density to determine which is most desirable. All the element densities at the beginning of the optimization process have the same value, the main objective is to drive the most desirable densities to 1 and meanwhile drive the others to a predefined minimum value which approach to 0.

Similar to the SIMP method, the CFAO method simultaneously set the element density and element fiber angle as design variables, the density allows the optimization of material layout distribution. Meanwhile, the fiber angle represents the optimized orientation of continuous fiber on the design domain. The fiber angles are often set as the same value at the beginning. The constraints on the angle design variables are set as  $-90^\circ$  to  $90^\circ$  or  $0^\circ$  to  $360^\circ$ . And the element fiber angle may increase or decrease according to the sensitivity in the optimization process and is driven to the most effective value. The fiber angle of each element can be continuously updated during the optimization process.

In the proposed Bi-CFAO, the element angles of two layers are set as design variables. And the two angles of each element are set as perpendicular, which represents the vertical orthogonality fiber paths of the two layers.

### 2.3 Optimization Model

In this paper, the IGA based Bi-CFAO method for compliance minimization under available volume constraint is considered. The corresponding problem formulation can be written as:

Find:  $\mathbf{x} = \{x_e\}$ ,  $\boldsymbol{\theta} = \{\theta_e\}$ , where  $e \in [1, n]$ .

Minimize:  $c(\mathbf{x}, \boldsymbol{\theta}) = \mathbf{U}^T \mathbf{K} \mathbf{U} = \sum_{e=1}^n (x_e)^q \mathbf{u}_e^T [k_e(\theta_e) + k_e(\theta'_e)] \mathbf{u}_e$

Subjected to:

$$V(x)/V_0 \leq f,$$

$$\mathbf{K} \mathbf{U} = \mathbf{F}$$

$$0 \leq x_e \leq 1, \quad -90^\circ \leq \theta_{\min} \leq \theta_e \leq \theta_{\max} < 90^\circ \quad (10)$$

where  $\mathbf{x}$  is the element density vector,  $\boldsymbol{\theta}$  is the element angle vector,  $n$  is the element number,  $c$  is the compliance,  $\mathbf{U}$ ,  $\mathbf{K}$  and  $\mathbf{F}$  are the global displacements, global stiffness matrix and force vectors, respectively,  $\mathbf{u}_e$  and  $k_e$  are the element displacement field and the element stiffness matrix,  $q$  is the penalization factor (set as 3 in this paper), which is similar with SIMP approach [12,13].  $V_0$  and  $f$  are the design domain volume and prescribed volume constraint fraction.  $\theta_{\min}$  and  $\theta_{\max}$  are respectively the lower and upper bound of the design variables  $\theta_e$ .

For numerical implementation purposes, as a common practice in the literature [13], a density filter transformation is often applied to avoid the checkerboard patterns. In the present work, the form of density filtering is taken as:

$$\bar{x}_e = \frac{1}{\sum_{i \in N_e} \mathbf{H}_{ei}} \sum_{i \in N_e} \mathbf{H}_{ei} x_i \quad (11)$$

where  $\bar{x}_e$  is the filtered density which is referred to as the physical element density of element  $e$  and updated by a set of element densities  $x_i$  which has the center-to-center distance smaller than the filter radius  $r_{\min}$ , and  $\mathbf{H}_{ei}$  is a weight factor defined as:

$$\mathbf{H}_{ei} = \max(0, r_{\min} - \varepsilon(e, i)) \quad (12)$$

where  $\varepsilon(e, i)$  is the distance between element  $e$  and  $i$ .

In the present study, the plane-stress quadrilateral element is used. The global stiffness matrix  $\mathbf{K}$  is obtained by assembling elemental stiffness matrices given by elemental stiffness matrices. The orthotropic material element stiffness matrix  $\mathbf{K}_e$  in CFAO method is different from the isotropic SIMP method:

$$\mathbf{K}_e(\theta_e) = \iint h \mathbf{B}^T [C_e(\theta_e) + C_e(\theta'_e)] \mathbf{B} d\Omega_e \quad (13)$$

where 2D integration is performed over each element domain  $\Omega_e$ ,  $h$  is the element thickness normal to the plane of the structure,  $\mathbf{B}$  is the strain-displacement matrix and  $C_e$  is the element orthotropic constitutive matrix,  $\theta_e$  and  $\theta'_e$  are element angles ( $\theta'_e = \theta_e \pm 90^\circ$ ). The elastic matrix for orthotropic material with angle  $\theta_e$  is defined as:

$$C_e(\theta_e) = T(\theta_e) C T(\theta_e)^T \quad (14)$$

where  $C$  is the original elastic matrix without rotation of fiber;  $T$  is the transformation matrix which is affected by fiber angle  $\theta_e$ . More details are referred to [10,34].

$$C = \frac{1}{1 - \nu_{xy}\nu_{yx}} \begin{bmatrix} E_x & \nu_{yx}E_x & 0 \\ \nu_{xy}E_y & E_y & 0 \\ 0 & 0 & G_{xy} \end{bmatrix} \quad (15)$$

$$T(\theta_e) = \begin{bmatrix} \cos^2\theta_e & \sin^2\theta_e & -2\cos\theta_e\sin\theta_e \\ \sin^2\theta_e & \cos^2\theta_e & 2\cos\theta_e\sin\theta_e \\ \cos\theta_e\sin\theta_e & -\cos\theta_e\sin\theta_e & \cos^2\theta_e - \sin^2\theta_e \end{bmatrix} \quad (16)$$

where  $E_x$  and  $E_y$  are the Young's modulus,  $G_{xy}$  is the shear modulus,  $\nu_{xy}$  and  $\nu_{yx}$  are the Poisson's ratios.

#### 2.4 Design Sensitivity Analysis

In the minimum compliance problems, the compliance sensitivity for an arbitrary geometry parameter can be written as:

$$\frac{\partial c}{\partial x_e} = -u^T \frac{\partial K}{\partial x_e} u = - \sum_{e=1}^n (q x_e^{q-1} u_e^T [k_e^s(\theta_e) + k_e^s(\theta'_e)] u_e) \quad (17)$$

The derivatives of  $c$  for the fiber angles are obtained as

$$\begin{aligned} \frac{\partial c}{\partial \theta_e} = -u^T \frac{\partial K}{\partial \theta_e} u = -x_e^q u_e^T \left\{ \iint_{\Omega_e} h \left( \mathbf{B}^T \left[ \frac{\partial T^{-1}}{\partial \theta_e} + \frac{\partial T^{-1}}{\partial \theta'_e} \right] C T^{-T} \mathbf{B} \right. \right. \\ \left. \left. + \mathbf{B}^T T^{-1} C \left[ \frac{\partial T^{-T}}{\partial \theta_e} + \frac{\partial T^{-T}}{\partial \theta'_e} \right] \mathbf{B} \right) d\Omega \right\} u_e \end{aligned} \quad (18)$$

The derivatives differ from element to element in the design domain, as the fiber angles are set as in element-level.

### 3 IGA Based Bi-CFAO Method

In this section, the IGA based optimization method for Bi-CFAO is addressed. In the isogeometric Bi-CFAO method, IGA is used to replace the general numerical computation method FEM. The NURBS basis functions (e.g., Eqs. (8) and (9)), which represent the CAD models, are directly used in structural analysis as shape functions in NURBS based IGA. Hence, a variable  $x$  (e.g., density, displacement, or force) whose parametric coordinate is  $(\xi, \eta)$  can be evaluated from the control point values

$$x(\eta, \xi) = \sum_i^n N_i(\eta, \xi) x_i \quad (19)$$

where  $x$  and  $N$  are the variable value and the basis function of  $i$ -th control point, respectively.

In terms of the NURBS interpolation, the element stiffness matrix  $\mathbf{K}_e$  can be constructed as

$$\mathbf{K}_e(\theta_e) = \iint hB^T [C_e(\theta_e) + C_e(\theta'_e)] B d\Omega_e = \iint hB^T [C_e(\theta_e) + C_e(\theta'_e)] B |J_1| |J_2| d\bar{\Omega}_e \quad (20)$$

where  $J_1$  and  $J_2$  are the transformation relationship that map integrals from the NURBS parametric space to the physical space, and from the integration parametric space to the NURBS parametric space respectively. More details are referred to [15,16,18,22,23], and [57].

### 3.1 Control-Point Based IGA in Bi-CFAO

Unlike the FEM method, the physical models in the IGA are represented by the NURBS basis functions in control points. And they are translated from the NURBS parametric space instead of the FEM Lagrange elements. The NURBS basis functions in the control-points are both used in the geometric models and structural analysis models. In the NURBS based IGA, the design variables can be set on the control points instead of setting on the element nodes, so that the topology optimization filed of the layout could be directly used in the CAD models. The sensitivities of the objective function  $c$  with respect to the control points are written as

$$\frac{\partial c}{\partial \tilde{x}_i} = \sum_{j \in e_i} \frac{\partial c}{\partial x_{e_{ij}}} \frac{\partial x_{e_{ij}}}{\partial \tilde{x}_i} = - \sum_{j \in e_i} q_{x_{e_{ij}}} q^{-1} u_{e_{ij}}^T [k_{e_{ij}}^s(\theta_e) + k_{e_{ij}}^s(\theta'_e)] u_{e_{ij}} \frac{\partial x_{e_{ij}}}{\partial \tilde{x}_i} \quad (21)$$

where  $\tilde{x}_i$  denotes the variable (i.e., density) of the  $i$ -th control point,  $e_i$  is the element set on which the  $i$ -th control point influences,  $e_{ij}$  is the  $j$ -th element of  $e_i$ . The derivation in the former chain derivation process can be calculated as

$$\frac{\partial x_{e_{ij}}}{\partial \tilde{x}_i} = \sum_{k \in e_j} N_i(kc) \quad (22)$$

where  $kc$  denotes the center of the  $k$ -th element in the element set  $e_j$  which is the  $j$ -th element influenced by the control point  $i$ , and  $N_i(kc)$  is the NURBS basis function of control point  $i$  corresponding to the center of element  $k$ .

### 3.2 Optimization Algorithm

In the present work, the well-known MMA optimizer [59] is adopted to solve the topology and angle optimization problems formulated in the former sections. The element stiffness matrices are calculated in the IGA progress, and the derivatives of the element stiffness matrix and the derivatives of structural compliance for fiber angles in every related control point are calculated in the design sensitivity progress.

The optimization process will be terminated when the convergence criterion is satisfied. In this paper, the convergence criterions are defined as the iteration number is larger than max iterations number  $N$  or the density and fiber angles of the current iteration is less than  $\delta$  ( $\delta$  is the preset convergence error, in this work  $\delta = 0.0001$ ).

## 4 Generate Fiber Path

### 4.1 Generate Fiber Path and Update the Fiber Angle

After the fiber angles are obtained by the optimization process, the fiber paths can be drawn in the MATLAB function stream slice. The sine and cosine of the element angles and the coordinates of the element center points are set as inputs. In this work, the fiber paths are generated as streamlines by the fiber angles. Because the fiber orientation at each arbitrary point is tangent to the fiber paths, the fiber path is similar to the streamline. The fiber path generation process can be implemented in other software as well, such as the *Tecplot* [60].

In this paper, the fiber paths in both two layers are generated. And it should be noted that the fiber path generation procedure can be performed during and after the optimization iterations to plot the fiber path results. In this work, the fiber paths are generated in every ten iterations to show the path updating with the optimization iterations. More details about the fiber paths generating and visualizing process are refer to references [60,61].

As discussed previously in [8,34] the optimized fiber angles in one layer may lead to local spatial discontinuities or other manufacturing conflicts such as large fiber path curvatures problems or fiber path flexibility problems. In this paper, the angles in two layers are considered as perpendicular orthogonal in the design domain. And it is found that, some of the local discontinuity may vanish if the angles are replaced by the angle results in the next layer. After the optimization process, an angle reselection process is performed to reduce the local discontinuities of the fiber paths. The procedure of fiber angle reselection progress is shown in Tab. 1.

**Table 1:** Algorithm for angle reselection procedure

Angle reselection procedure		
$i, j, k, l$ : counter	$r, r_{new}$ : minimal curvature radius	$Idx\_s$ : index of max size
$L, L_{f1}, L_{f2}, L_{new}$ : fiber paths	$n$ : number of elements	$aa$ : average of angles
$X, Y$ : element coordinates	$ag$ : angle groups	$jc$ : judgement criterion
$a, a_{new}$ : element angles	$s$ : angle group size	$idx\_a$ : index of reselected angles
1: $i = 0, l = 0$		
2: $streamslice(X, Y, a) \Rightarrow L, [L_{f1}] \Leftarrow fit(L), [r] \Leftarrow curvature\_radius(L_{f1})$		
3: for $j = 1: n, [ag] \Leftarrow classify\_angles(a)$ , end		
4: for $k = 1:4, size(find(ag==k)) \Rightarrow s(k), \max(s) \Rightarrow idx\_s$ , end		
5: $mean(a(idx\_s)) \Rightarrow aa$		
6: $find((a - aa) > jc) \Rightarrow idx\_a, a(idx\_a) + 90^\circ \Rightarrow a_{new}(idx\_a)$		
7: $find(a_{new} > 90^\circ) \Rightarrow idx\_a, a_{new}(idx\_a) - 180^\circ \Rightarrow a_{new}(idx\_a)$		
8: $streamslice(X, Y, a_{new}) \Rightarrow L_{new}, [L_{f2}] \Leftarrow fit(L_{new}), [r_{new}] \Leftarrow curvature\_radius(L_{f2})$		
9: while $i < 5$ and $l < 1$		
10: if $mean(r_{new}) > mean(r)$		
11: $l = 1,$		
12: else		
13: $l = 0, i = i + 1, a = a + 45^\circ$ , go to 2		
14: end		
15: end		

The variables are explained in the upper lines, as shown in Tab. 1. The double line arrow  $\Rightarrow/\Leftarrow$  represent the Matlab functions and the user-defined functions respectively. As show in Tab. 1, there are three user-defined functions:  $fit$ ,  $curvature\_radius$ , and  $classify\_angles$ .

Firstly, initialize the counter  $i$  and  $l$ . Then generate the fiber paths using the function  $streamslice$  in Matlab. After that the user-defined function  $fit$  is performed to generate the fit equations of the paths. In the  $fit$  function, quadratic polynomial equations are used. And then the fitted equations are used to

calculate the minimal curvature radius in the *curvature\_radius* function. After that, the *classify\_angles* function *classifies* the fiber angles to 4 groups (a. Horizontal ( $\theta_e \in (-22.5^\circ, 22.5^\circ)$ ), b. Vertical ( $\theta_e \in [67.5^\circ, 90^\circ)$  or  $\theta_e \in [-90^\circ, -67.5^\circ]$ ), c. Oblique up ( $\theta_e \in [22.5^\circ, 67.5^\circ)$ ), d. Oblique down ( $\theta_e \in (-67.5^\circ, -22.5^\circ]$ ), according to the directions of the fibers.

The variable *ag* represents the index of the angle groups. The fourth line returns the max size of the four angle groups *s*. And the fifth line finds the average of angles in the angle groups *idx\_s*. The sixth line get the element angles which should be updated according to the difference between the fiber angles of element and the average value of the *s* angles. If the difference between the fiber angles is bigger than *jc*, then the angle is added with  $90^\circ$ . The angle bound *jc* in this paper is set as  $67.5^\circ$ . After updating, the new angles should be updated in the range of  $[-90^\circ, 90^\circ)$ . If the angle is out of this range, then add  $180^\circ$  or  $-180^\circ$ . After this step, the minimal curvature radii of the new paths are calculated in line 8. If the average value of minimal curvature radii of the new paths  $r_{new}$  is bigger than *r*, then output the new paths. Otherwise, the same updating progress will be performed with the initial angles adding  $45^\circ$  and  $-45^\circ$ , the angles are updated according to the new angles. After this step, the reselection progress will be terminated.

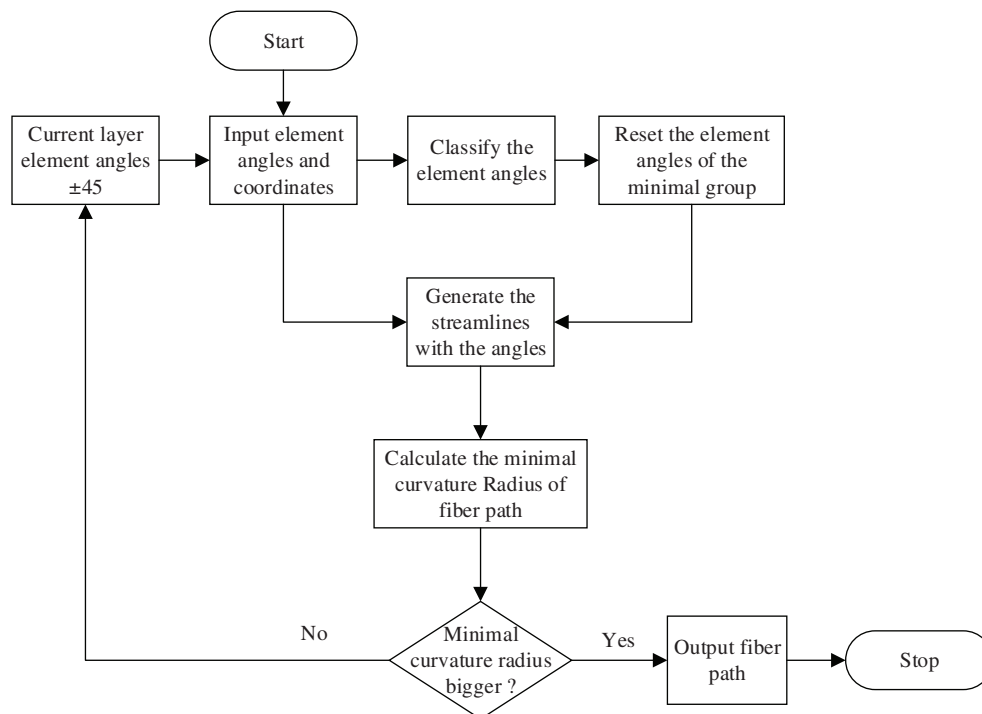


**Figure 1:** The flowchart of angle reselection procedure

The angle reselection procedure can be performed during or after the optimization iteration process. And the flowchart of angle reselection procedure is shown in Fig. 1. It should be noted that this angle reselection procedure may reduce the angle local discontinuity problem, but the effectiveness cannot be guaranteed.

#### 4.2 Optimization Procedure

The evolution procedure of the IGA Bi-CFAO is similar to the conventional SIMP based CFAO, but the mechanics analysis is implemented by the NURBS-based IGA, and the density sensitivity numbers are based on the NURBS control points, the fiber angles of two layers are set as perpendicular orthogonal and the current layer angles are set as design variables as well as the densities.

The optimization procedure can be outlined as follows:

- Step 1. Define optimization parameters such as target volume  $V_0$ , penalization parameter  $q$ .
- Step 2. Set up material properties such as Young's modulus  $E_x, E_y$  and Poisson's ratio  $\nu_{xy}$ , and boundary conditions such as forces and supports.
- Step 3. Generate NURBS spaces for IGA.
- Step 4. Analyze the structural response by IGA based on NURBS spans (an IGA span is similar to an element defined in FEM) (Section 2.3).
- Step 5. Calculate the sensitivity numbers of NURBS based control points (Eq. (21)).
- Step 6. Update the design variables using the MMA optimization process, i.e., the densities and the fiber angles on the control points.
- Step 7. Repeat Steps 4–6 until the objective volume  $V_0$  and the convergence criterion are satisfied.

Fig. 2 shows the flowchart corresponding to the above procedure.

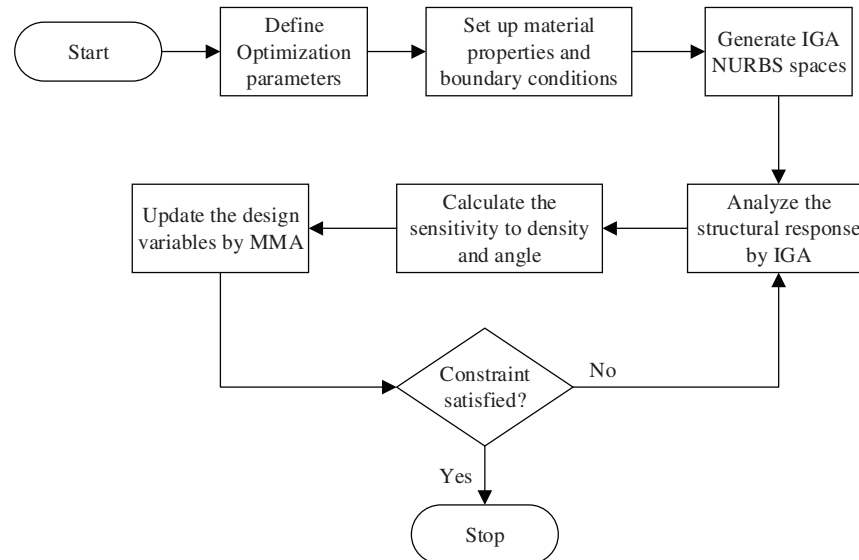


**Figure 2:** The flowchart of IGA based Bi-CFAO optimization procedure

## 5 Examples

Numerical examples of minimal compliance optimization problems are presented to demonstrate the characteristics of the IGA based Bi-CFAO method. The domain integration scheme defined by Eqs. (18) and (21) is used to evaluate the design sensitivities.

All the examples are run on a laptop: the CPU is an Intel core i7 10710U 1.6 GHz, the RAM is 16 GB, the OS is Windows 10, and the software environment in MATLAB R2015a. The Young's modulus for the composite material is  $E_x = 1.0$ ,  $E_y = 0.1$  and the Poisson's ratio is 0.36. For simplicity, the target volume is set as  $V_0 = 0.8$ . A Gauss quadrature rule of  $3 \times 3$  is used for quadratic IGA elements. And the conventional 9 nodes quadratic finite element is used to perform FEM computing.

### 5.1 Cantilever Beam

The first numerical example is the short cantilever beam design problem, which is one of the most used benchmark topology optimization problems. It is used to verify the effectiveness of the proposed Bi-CFAO

method compared to conventional design approaches. The design domain is a  $W \times H$  rectangle with a concentrated force located at the midpoint of the right side,  $W = 2$  m,  $H = 1$  m, and it is shown in Fig. 3. In this paper, the design domain has meshed in different sizes to compare the calculation efficiency between IGA and FEM.

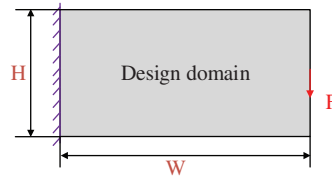


**Figure 3:** Design domain with boundary conditions and dimensions of the cantilever beam

The calculation efficiency is here measured by the average time at each step, as shown in Tab. 2. The results show that the speedup of IGA/FEM ranges from 2.8 to 4.5, values prove the higher efficiency of the IGA method, which meets the results presented by literatures [15–17,22]. It should be noted that both of mechanical property evaluation procedures and structure response analysis procedures for IGA and FEM are different and are compared in this paper. The computational costs of other CFAO procedures such as the sensitivity analysis and variable updating procedures are the same and they are not counted in this comparison.

**Table 2:** Compare of calculating efficiency between IGA and FEM by the average time of each optimization iteration

Cases	DOFs of FEM	DOFs of IGA	FEM time (s)	IGA time (s)	Speed up
$16 \times 8$	1122	360	0.34	0.12	2.8
$32 \times 16$	4290	1224	1.39	0.43	3.2
$64 \times 32$	18,354	4488	9.3	2.75	3.4
$128 \times 64$	69,426	17,160	89.2	30.3	2.9
$256 \times 128$	269,874	67,080	1787.0	395.4	4.5

The Convergence history of the objective function and the volume ratio over the iterations are shown in Fig. 4. The objective function value is larger during the initial iterations and it decreases rapidly in the former 20 iterations. The element density converges fast and the material distribution almost invariable after about 40 iterations.

The fiber angle updating history of Bi-CFAO and the conventional CFAO method are presented in Tab. 3. The results in the 1st, 40th, 100th iterations are listed for simplicity. The results for CFAO are listed in the first column, the fiber angles in the other layer are the same as this layer. The results for Bi-CFAO are listed as the three columns. The former two columns represent the first and second layers, respectively. The third column represents the mixed results of the two layers. It is easy to find that the fiber angles in both Bi-CFAO and method are mostly continuous in the design domain, but locally discontinuous exist in both two methods (shown in 40th and 100th fiber angles).

The fiber paths are generated by MATLAB and the results show that the fiber paths are more neat and smoother in Bi-CFAO than conventional CFAO. The fiber paths in the 1st layer in BI-CFAO in the last iteration is compared with the result in conventional CFAO (the former two images in the last row in Tab. 3), to compare the two methods under the same conditions.

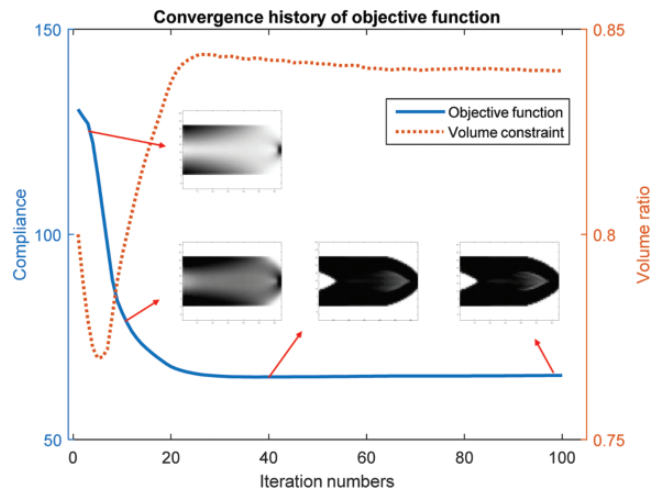


**Figure 4:** Convergence history of the objective function of the cantilever beam

**Table 3:** Comparison of fiber angles and paths obtained by CFAO and Bi-CFAO optimization iteration

Iterations	CFAO	Bi-CFAO, 1st Layer	Bi-CFAO, 2nd Layer	Bi-CFAO, 2 Layers
1				
40				
100				

The minimum curvature radii of all the fiber paths are calculated using the streamlines shown in Tab. 3. and the results are shown in Fig. 5. The  $x$  values  $x_i$  are the normalization of the minimum curvature radius values ( $y_i$ ). The normalization expression is  $x_i = (y_i - \min(y_i)) / (\max(y_i) - \min(y_i)) \times 10$ . The average value of the minimum curvature radii obtained by Bi-CFAO is 83.3, meanwhile, the average value by CFAO is 32.9. The minimum value of the paths is 8.2 and 1.2 by Bi-CFAO and CFAO, respectively. The improvement rate is 2.5 and 6.8, respectively. It is noted that the curvature varies from point to point in the same fiber path. Some local sharp points are found in the paths while most of the points are smooth in the paths. These local sharp points may impact the calculation of the minimum curvature radius. The improvement of the smoothness of the fibers meets the need of the manufacturing process.

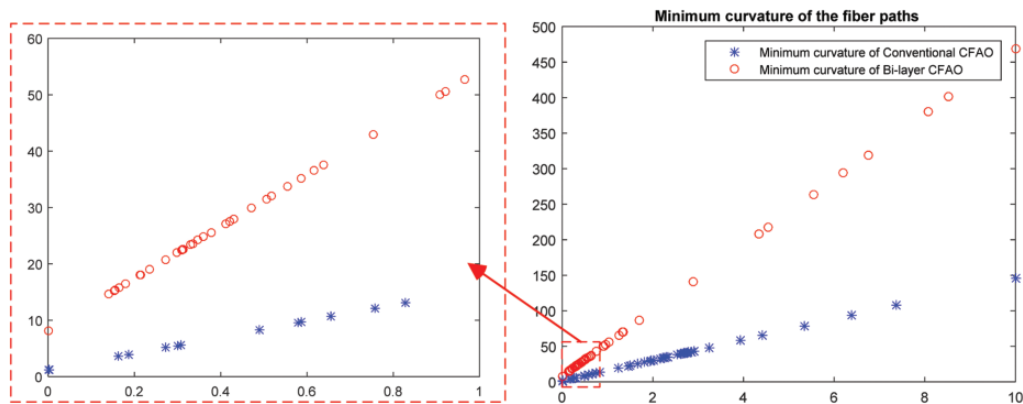


**Figure 5:** The minimum curvature for all the fiber paths in CFAO and Bi-CFAO

Fig. 6 shows the convergence history of the objective function with the two methods. The volume constraints are both set as 0.8, and the element stiffness matrix is calculated using two perpendicular orthogonal layers which are described in the former sections. The element stiffness matrix in Bi-CFAO utilizes the mean value of the two-element stiffness matrices of the 2 layers ( $Ke = 0.5 * (Ke_{\theta_e} + Ke_{\theta_e+90^\circ})$ ), to compare the two methods under the same conditions. The objective function obtained by Bi-layer fiber angles  $(\theta_e$  and  $\theta_e')/2$  are compared with two identical layer fiber angles  $(\theta_s$  and  $\theta_s')/2$ . Where the element fiber angles  $\theta_e$  and  $\theta_e'$  are the two-layer element fiber angles in Bi-CFAO, and  $\theta_s$  represents the single-

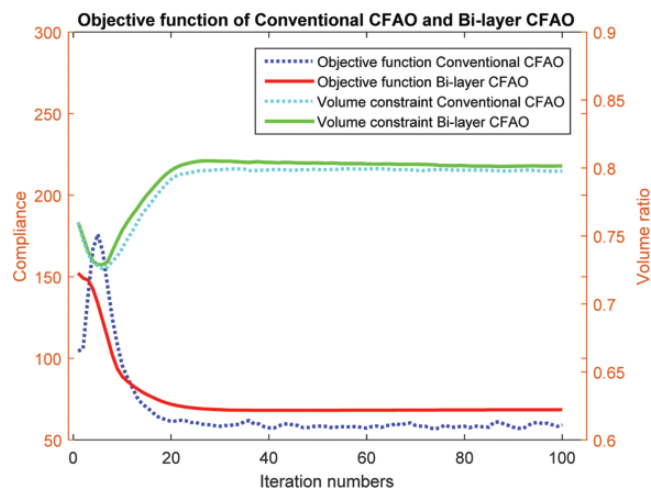


**Figure 6:** Convergence history of the objective function with CFAO and Bi-CFAO of the cantilever beam

layer fiber angles in CFAO. It is found that the objective function is 68.1 in Bi-CFAO, and the value is 56.8 in CFAO method. The structure compliance in Bi-CFAO is bigger than CFAO and the drawback is 19.9%. It is roughly attributable to the focusing optimization of each element angle in a single layer while almost half of the Bi-layer angles are not.

The advantage of Bi-CFAO is the smoother fiber path, which can improve structural performance. It is not modeled in the composite structure response calculation process in this paper because a higher fidelity modeling method considering accurate modeling fiber-matrix structures is needed. The profit and loss of the double-layer fiber angle optimization results may be compensated when a higher fidelity model is utilized.

Fig. 7 shows the fiber angle and fiber path results obtained through the proposed optimization method starting from different initial fiber angle arrangements, i.e.,  $\theta_{el}^0 = 0^\circ$  and  $\theta_{el}^0 = 90^\circ$ . The optimized fiber angles and the final fiber paths of the two models differ from one to another. The obtained fiber paths are almost identical except for some paths in partial domains. The objective functions of the two models are not significant. Meanwhile, the maximum curvature and uniformity of the fiber paths are almost the same in most parts of the design domain and different in partial domains.

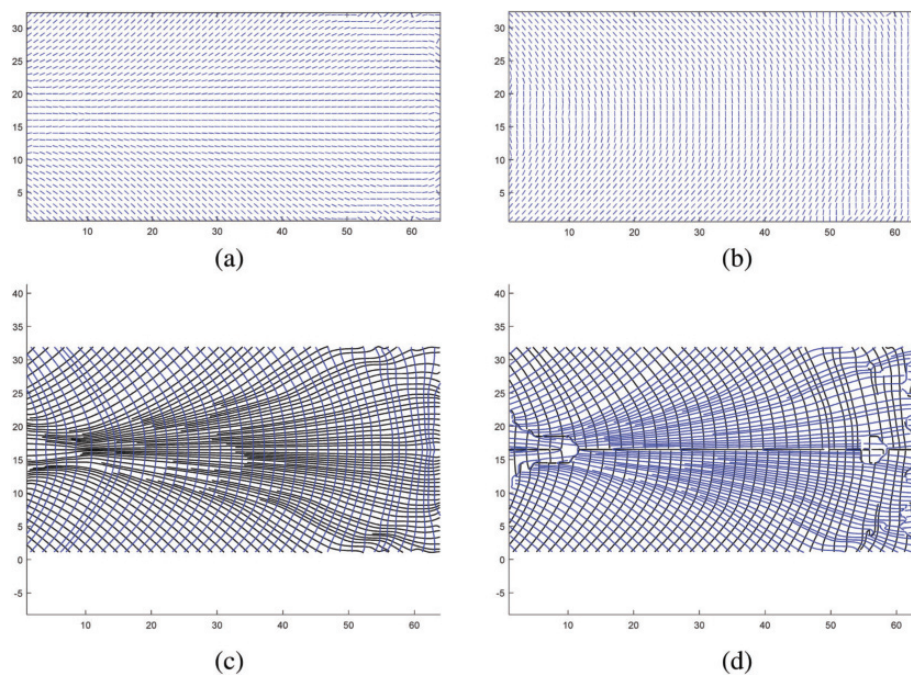


**Figure 7:** Initial fiber angle arrangement of cantilever beam (a) Fiber angle result of  $0^\circ$  (b) Fiber angle result of  $90^\circ$  (c) Fiber path result of  $0^\circ$  (d) Fiber path result of  $90^\circ$

## 5.2 MBB Beam

The Messerschmidt-Bolkow-Blohm (MBB) beam problem is another commonly used benchmark problem for topology optimization methods. MBB beam is a simply supported beam subject to a vertical force at the middle point of the bottom sideline. Due to symmetry, only half MBB beam is modeled and symmetry boundary conditions are applied. The design domain is a  $W \times H$  rectangle, in this paper  $W = 2$  m,  $H = 1$  m, which is shown in Fig. 8.

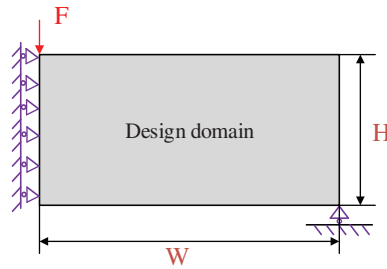


**Figure 8:** MBB beam design domain

In Fig. 9, the convergence history of objective functions is presented. The density of all the elements which represent the material distribution renovated rapidly in the former 40 iterations. In the last 60 iterations, the updating of the fiber angles and element densities changes not obviously.

The fiber angle updating history in the 1st, 40th, 100th iterations of Bi-CFAO and the conventional CFAO method are presented in Tab. 4. The fiber angles in both Bi-CFAO and method are mostly continuous in the design domain, but locally discontinuous exist in both two methods (shown in 40th and 100th fiber angles). It is found that the local discontinuity in CFAO are more serious than the results in Bi-CFAO.

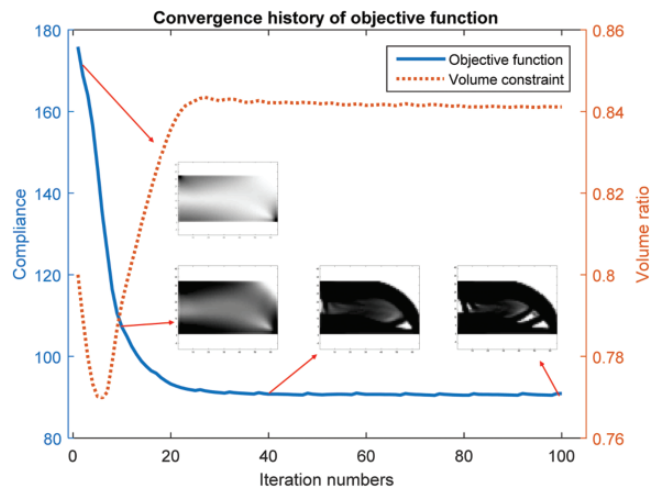


**Figure 9:** Convergence history of the objective function of MBB beam

The fiber paths are generated and the results show that the fiber paths are more neat and smoother in Bi-CFAO than conventional CFAO. The fiber paths in the 1st layer in BI-CFAO in the last iteration is compared with the result in conventional CFAO (the former two images in the last row in Tab. 4), to compare the two methods under the same conditions.

The minimum curvature radius values are shown in Fig. 10. The average value of the minimum curvature radius obtained by Bi-CFAO is 552.1, meanwhile, the average value by CFAO is 29.9. The minimum value of the paths is 1.68 and 0.18 by Bi-CFAO and CFAO, respectively. The improvement rate is 18.5 and 9.3, respectively. It is noted that the max curvature radius obtained in the bottom-left corner in the design domain where the fiber paths are approximately straight lines. More sharp turns are found in the fiber paths in CFAO. The fiber paths in Bi-CFAO are smoother and neater than the single-layer CFAO, which is beneficial to reduce the performance damage due to manufacturing.

**Table 4:** Comparison of fiber angles and paths MBB beam

Iterations	CFAO	Bi-CFAO, 1st Layer	Bi-CFAO, 2nd Layer	Bi-CFAO, 2 Layers
1				
40				
100				

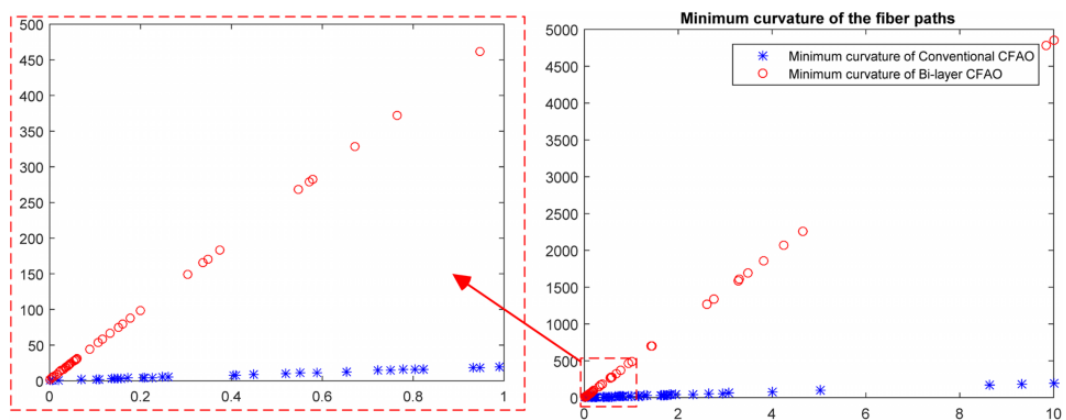


**Figure 10:** The minimum curvature for all the fiber paths in CFAO and Bi-CFAO MBB beam

The comparison of the objective function of MBB beam is shown in Fig. 11. It is found that the objective function is 83.4 Bi-CFAO, and the value 58.5 in CFAO method. The objective function is bigger than CFAO method and the drawback is 42.6%. The differences of fiber path shapes between Bi-CFAO and CFAO are significant meanwhile the smoothness quality cannot be guaranteed in CFAO. It shows that the objective function and the smoothness are two contradictory characters, the fiber paths in CFAO are located in the most effective position but their curvature is bigger than Bi-CFAO. The fiber paths in Bi-CFAO are smooth but the objective function is worse than CFAO. This is roughly because the objective functions are calculated considered no manufacturing constraints.

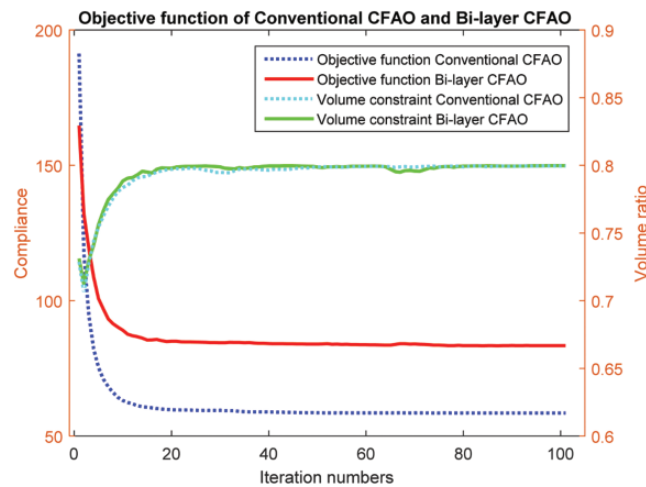


**Figure 11:** Convergence history of the objective function with CFAO and Bi-CFAO of MBB beam

Fig. 12 shows the fiber angle and fiber path results obtained through different initial fiber angle arrangements, i.e.,  $\theta_{el}^0 = 0^\circ$  and  $\theta_{el}^0 = 90^\circ$ . The optimized fiber angles and the final fiber paths of the two models differ from one to another. Most of the shapes of the fibers are the same while the fibers are different in a few partial domains. Which implies that the optimization is not dependent on the initial designs, the initial fiber angles do have limited impact with the path qualities.

### 5.3 Quarter Annulus

This example is a benchmark TO problem which is always been utilized in NURBS based IGA topology optimization both in LSM, SIMP and BESO framework. The design domain is a quarter annulus with curved boundaries and the inner radius  $r = 1$  m and outer radius  $R = 2$  m which is shown in Fig. 13. The edge in the bottom is fixed and a concentrated force  $F$  is horizontally loaded at the left-top corner. In this example, the element angle and density are optimized with both FEM and IGA method. And the efficiency of these two methods are compared.

The element size is  $32 \times 32$  and the convergence history of objective function and volume constraint is shown in Fig. 14. The process of density convergence is similar to the previous examples. After 40 iterations the element density and the structure layout change little and the objective function remains stable.

The comparison of the two methods are shown in Fig. 15. The fiber angles obtain by the two methods are different. And the results shown in (c) and (d) are mostly consecutive in both of the design domain. The discontinuity of the fiber paths (local area with larger curvature fiber path in the design domain) appears in both of the two methods. And similar to the former examples, the uniformity and smoothness of fiber paths are improved when Bi-CFAO is used.

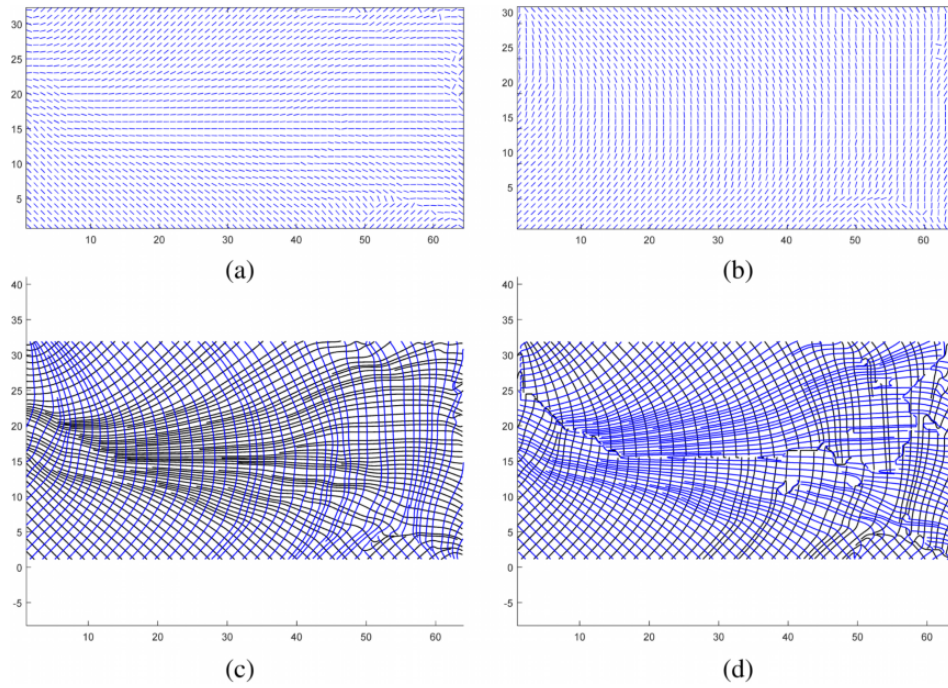


**Figure 12:** Initial fiber angle arrangement of MBB beam. (a) Fiber angle result of  $0^\circ$  (b) Fiber angle result of  $90^\circ$  (c) Fiber path result of  $0^\circ$  (d) Fiber path result of  $90^\circ$

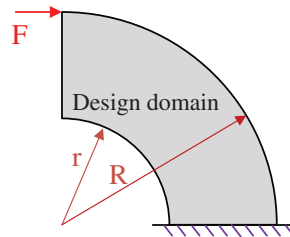


**Figure 13:** Quarter annulus design problem

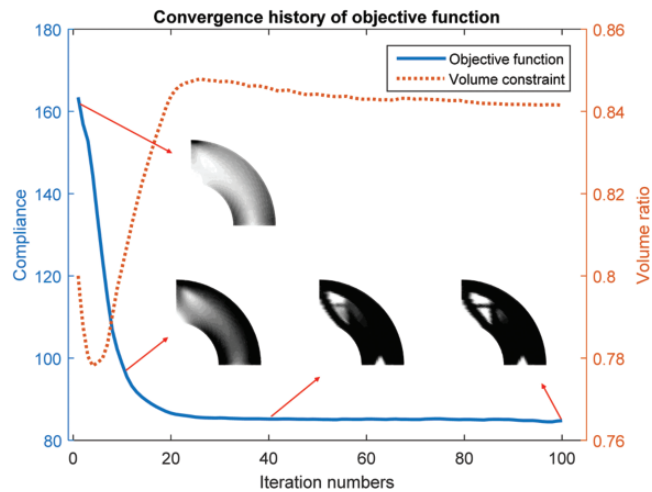


**Figure 14:** Convergence history of the objective function quarter annulus

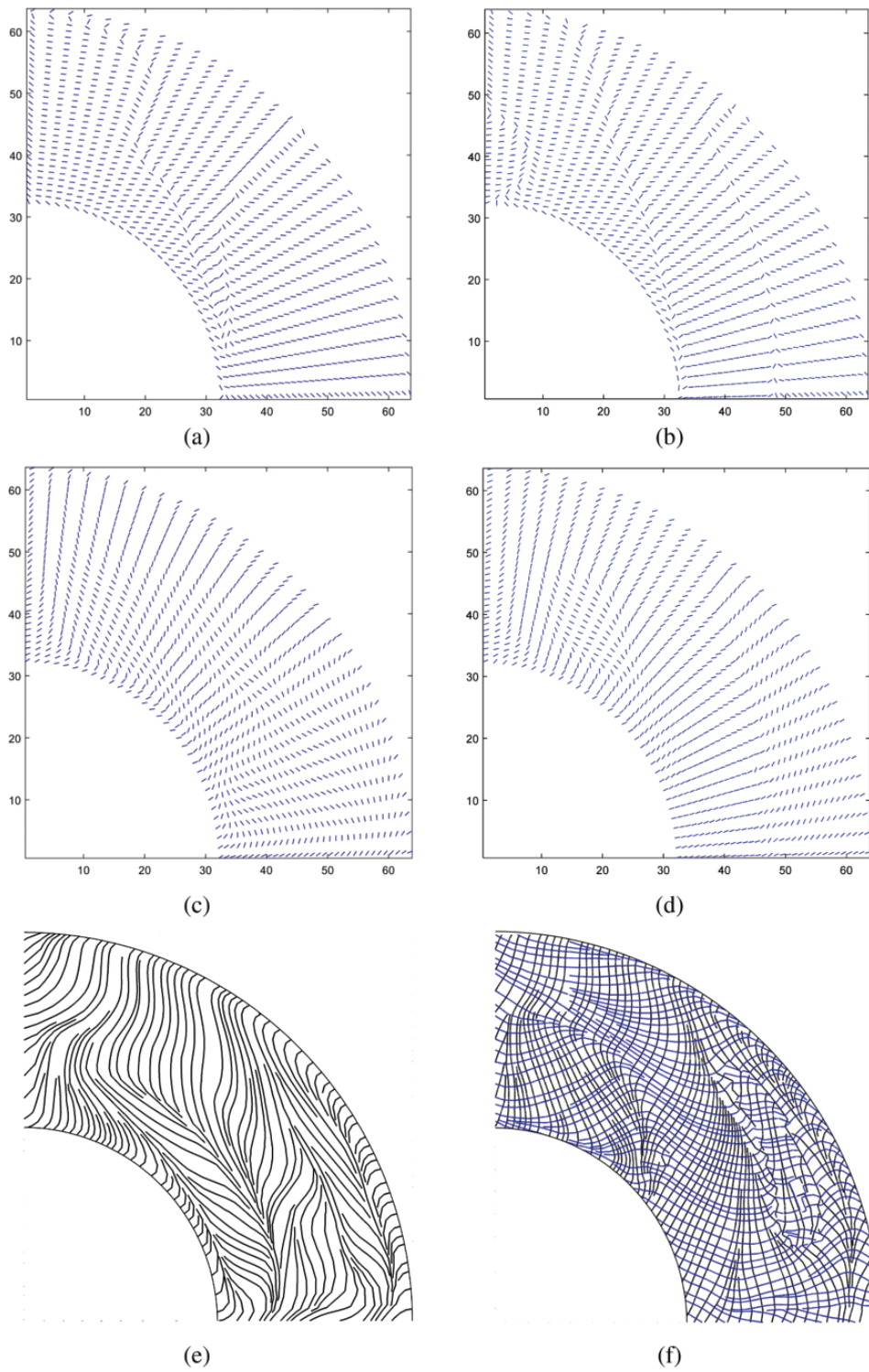


**Figure 15:** Angles and fiber paths of Conventional CFAO and Bi-CFAO of the quarter annulus. (a) CFAO angles 1st iteration. (b) Bi-CFAO angles 1st iteration. (c) CFAO angles final iteration. (d) Bi-CFAO angles final iteration. (e) CFAO paths. (f) Bi-CFAO paths

Fig. 16 shows the impact of the initial fiber angle arrangement on the final results of fiber angles and fiber paths. It is shown that the initial fiber angle arrangement may lead to little different optimized fiber angles in the design domain. From Figs. 16(c) and 16(d), the final fiber paths differ in partial parts of the design domain, but it is also easy to find that in the two results the fiber shapes in most domains are similar to each other. Further investigation on how to obtain a smoother fiber path according to different optimized fiber angles is needed, and it is vital when manufacturing constraints are considered.

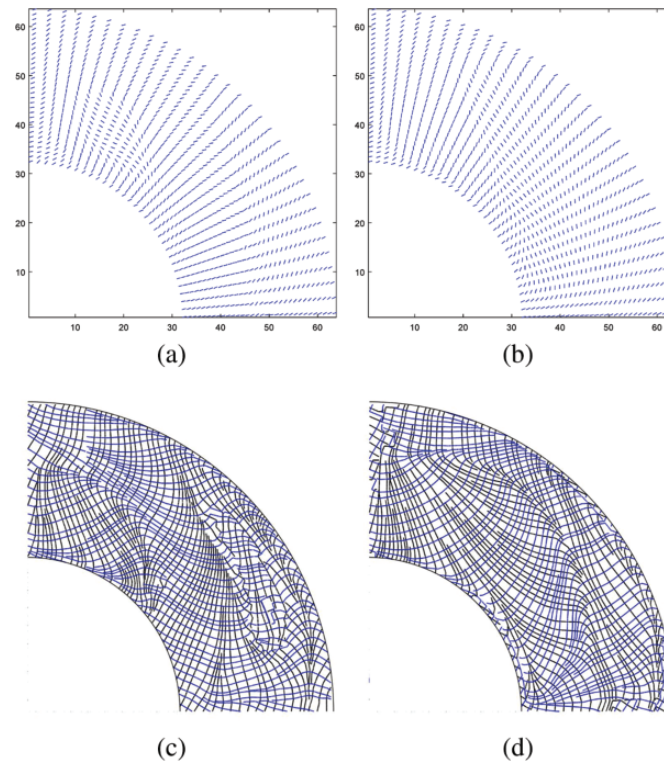


**Figure 16:** Initial fiber angle arrangement of the quarter annulus. (a) Fiber angle result of  $0^\circ$  (b) Fiber angle result of  $90^\circ$  (c) Fiber path result of  $0^\circ$  (d) Fiber path result of  $90^\circ$

## 6 Conclusion and Future Research

In this paper, we propose an IGA based topology and material orientation optimization method to simultaneously optimize the topology and fiber angles of the composite structure. In the proposed method, the sensitivity numbers for both densities and angles are calculated based on the NUBRS control points. The structural response analysis is performed by the IGA. For verifying the efficiency of calculation, the NURBS-based IGA method is compared with the quadratic finite element method (9 nodes). The computing cost of the structure response analysis and the sensitivities analysis are contained in the statistics. Three benchmark problems are performed to demonstrate the effectiveness of this method. The IGA based Bi-CFAO method assisted by NURBS shows significant speedup compared with the FEM (2.8 to 4.5 in the related cases).

The fiber angles obtained by the Bi-CFAO and conventional CFAO are compared. The fiber angles are utilized to generate fiber paths. The angle reselection procedure is used to investigate the smoothness of the optimized angles by calculating the minimum curvature radius of the paths. The minimum curvature radii of the fiber paths are calculated. It is found that the minimum radii obtained by the Bi-CFAO method are bigger

than that obtained by the CFAO. Meanwhile, the objective function values of the Bi-CFAO are bigger than that of CFAO. The influence of initial fiber angle values is presented by the numerical examples. It is found that the proposed method is stable. The NURBS based Bi-CFAO method is efficient for structure response analysis, topology optimization and fiber angle optimization. Smooth fiber paths with big curvature radii can be obtained by the proposed method.

Future research will focus on using the IGA based high fidelity numerical structure response analysis to deal with the inaccurate fiber-matrix modeling problem. Since the examples in this paper are all simple shapes, the future study can be extended to the design domain with arbitrary holes or other complex shapes. Although in this paper, only the minimum compliance problem is settled, the proposed Bi-CFAO method will not be restricted to this specific problem. The proposed Bi-CFAO method can be extended to deal with other problems, such as compliant mechanism problems [23] and Buckling optimization problems [38,40,62]. Moreover, the proposed method can be further improved in many aspects: e.g., using parallel computing with GPU or MPI to accelerate the IGA based angle optimization process [63].

**Funding Statement:** This research work is supported by the National Key R & D Project of China (Grant No. 2018YFB1700803, and Grant No. 2018YFB1700804) received by Qifu Wang.

**Conflicts of Interest:** The authors declare that they have no conflicts of interest to report regarding the present study.

## References

1. Ghiasi, H., Fayazbakhsh, K., Pasini, D., Lessard, L. (2010). Optimum stacking sequence design of composite materials part II: variable stiffness design. *Composite Structures*, 93(1), 1–13. DOI 10.1016/j.compstruct.2010.06.001.
2. Ghiasi, H., Pasini, D., Lessard, L. (2009). Optimum stacking sequence design of composite materials part I: constant stiffness design. *Composite Structures*, 90(1), 1–11. DOI 10.1016/j.compstruct.2009.01.006.
3. Gürdal, Z., Olmedo, R. (1993). In-plane response of laminates with spatially varying fiber orientations—variable stiffness concept. *AIAA Journal*, 31(4), 751–758. DOI 10.2514/3.11613.
4. Gürdal, Z., Tatting, B. F., Wu, C. K. (2008). Variable stiffness composite panels: effects of stiffness variation on the in-plane and buckling response. *Composites Part A: Applied Science and Manufacturing*, 39(5), 911–922. DOI 10.1016/j.compositesa.2007.11.015.
5. Xu, Y., Zhu, J., Wu, Z., Cao, Y., Zhao, Y. et al. (2018). A review on the design of laminated composite structures: constant and variable stiffness design and topology optimization. *Advanced Composites and Hybrid Materials*, 1(3), 460–477. DOI 10.1007/s42114-018-0032-7.
6. Esposito, L., Cutolo, A., Barile, M., Lecce, L., Mensitieri, G. et al. (2019). Topology optimization-guided stiffening of composites realized through automated fiber placement. *Composites Part B: Engineering*, 164, 309–323. DOI 10.1016/j.compositesb.2018.11.032.
7. Hao, P., Feng, S., Zhang, K., Li, Z., Wang, B. et al. (2018). Adaptive gradient-enhanced Kriging model for variable-stiffness composite panels using Isogeometric analysis. *Structural and Multidisciplinary Optimization*, 58(1), 1–16. DOI 10.1007/s00158-018-1988-1.
8. Kiyono, C. Y., Silva, E. C. N., Reddy, J. N. (2017). A novel fiber optimization method based on normal distribution function with continuously varying fiber path. *Composite Structures*, 160, 503–515. DOI 10.1016/j.compstruct.2016.10.064.
9. Luersen, M. A., Steeves, C. A., Nair, P. B. (2015). Curved fiber paths optimization of a composite cylindrical shell via Kriging-based approach. *Journal of Composite Materials*, 49(29), 3583–3597. DOI 10.1177/0021998314568168.
10. Nomura, T., Dede, E. M., Lee, J., Yamasaki, S., Matsumori, T. et al. (2015). General topology optimization method with continuous and discrete orientation design using isoparametric projection. *International Journal for Numerical Methods in Engineering*, 101(8), 571–605. DOI 10.1002/nme.4799.

11. Setoodeh, S., Abdalla, M. M., Gürdal, Z. (2005). Combined topology and fiber path design of composite layers using cellular automata. *Structural and Multidisciplinary Optimization*, 30(6), 413–421. DOI 10.1007/s00158-005-0528-y.
12. Bendsoe, M. P., Kikuchi, N. (1988). Generating optimal topologies in structural design using a homogenization method. *Computer Methods in Applied Mechanics and Engineering*, 71(2), 197–224. DOI 10.1016/0045-7825(88)90086-2.
13. Andreassen, E., Clausen, A., Schevenels, M., Lazarov, B. S., Sigmund, O. (2011). Efficient topology optimization in MATLAB using 88 lines of code. *Structural and Multidisciplinary Optimization*, 43(1), 1–16. DOI 10.1007/s00158-010-0594-7.
14. Meng, L., Zhang, W., Quan, D., Shi, G., Tang, L. et al. (2019). From topology optimization design to additive manufacturing: today's success and tomorrow's roadmap. *Archives of Computational Methods in Engineering*, 26, 1–26.
15. Wang, Y., Benson, D. J. (2015). Multi-patch nonsingular isogeometric boundary element analysis in 3D. *Computer Methods in Applied Mechanics and Engineering*, 293, 71–91. DOI 10.1016/j.cma.2015.03.016.
16. Wang, Y., Benson, D. J. (2016). Isogeometric analysis for parameterized LSM-based structural topology optimization. *Computational Mechanics*, 57(1), 19–35. DOI 10.1007/s00466-015-1219-1.
17. Wang, Y., Benson, D. J. (2016). Geometrically constrained isogeometric parameterized level-set based topology optimization via trimmed elements. *Frontiers of Mechanical Engineering*, 11(4), 328–343. DOI 10.1007/s11465-016-0403-0.
18. Wang, Y., Wang, Z., Xia, Z., Poh, L. H. (2018). Structural design optimization using isogeometric analysis: a comprehensive review. *Computer Modeling in Engineering and Sciences*, 117(3), 455–507. DOI 10.31614/cmcs.2018.04603.
19. Stegmann, J., Lund, E. (2005). Nonlinear topology optimization of layered shell structures. *Structural and Multidisciplinary Optimization*, 29(5), 349–360. DOI 10.1007/s00158-004-0468-y.
20. Stegmann, J., Lund, E. (2005). Discrete material optimization of general composite shell structures. *International Journal for Numerical Methods in Engineering*, 62(14), 2009–2027. DOI 10.1002/nme.1259.
21. Wang, Y., Liao, Z., Shi, S., Wang, Z., Poh, L. H. (2020). Data-driven structural design optimization for petal-shaped auxetics using isogeometric analysis. *Computer Modeling in Engineering & Sciences*, 122(2), 433–458.
22. Wang, Y., Benson, D. J., Nagy, A. P. (2015). A multi-patch nonsingular isogeometric boundary element method using trimmed elements. *Computational Mechanics*, 56(1), 173–191. DOI 10.1007/s00466-015-1165-y.
23. Wang, Y., Liao, Z., Ye, M., Zhang, Y., Li, W. et al. (2020). An efficient isogeometric topology optimization using multilevel mesh, MGCG and local-update strategy. *Advances in Engineering Software*, 139, 102733. DOI 10.1016/j.advengsoft.2019.102733.
24. Cai, S., Zhang, W., Zhu, J., Gao, T. (2014). Stress constrained shape and topology optimization with fixed mesh: a B-spline finite cell method combined with level set function. *Computer Methods in Applied Mechanics and Engineering*, 278, 361–387. DOI 10.1016/j.cma.2014.06.007.
25. Meng, L., Zhang, W. H., Zhu, J. H., Xu, Z., Cai, S. H. (2016). Shape optimization of axisymmetric solids with the finite cell method using a fixed grid. *Acta Mechanica Sinica*, 32(3), 510–524. DOI 10.1007/s10409-015-0549-8.
26. Kennedy, G. J., Martins, J. R. R. A. (2013). A laminate parametrization technique for discrete ply-angle problems with manufacturing constraints. *Structural and Multidisciplinary Optimization*, 48(2), 379–393. DOI 10.1007/s00158-013-0906-9.
27. Bruyneel, M. (2011). SFP—a new parameterization based on shape functions for optimal material selection: application to conventional composite plies. *Structural and Multidisciplinary Optimization*, 43(1), 17–27. DOI 10.1007/s00158-010-0548-0.
28. Bruyneel, M., Fleury, C. (2002). Composite structures optimization using sequential convex programming. *Advances in Engineering Software*, 33(7), 697–711. DOI 10.1016/S0965-9978(02)00053-4.
29. Gao, T., Zhang, W., Duysinx, P. (2012). A bi-value coding parameterization scheme for the discrete optimal orientation design of the composite laminate. *International Journal for Numerical Methods in Engineering*, 91(1), 98–114. DOI 10.1002/nme.4270.

30. Gao, T., Zhang, W., Duysinx, P. (2013). Simultaneous design of structural layout and discrete fiber orientation using bi-value coding parameterization and volume constraint. *Structural and Multidisciplinary Optimization*, 48(6), 1075–1088. DOI 10.1007/s00158-013-0948-z.
31. Zhou, Y., Nomura, T., Saitou, K. (2018). Multi-component topology and material orientation design of composite structures (MTO-C). *Computer Methods in Applied Mechanics and Engineering*, 342, 438–457. DOI 10.1016/j.cma.2018.07.039.
32. Weldeyesus, A. G., Stolpe, M. (2016). Free material optimization for laminated plates and shells. *Structural and Multidisciplinary Optimization*, 53(6), 1335–1347. DOI 10.1007/s00158-016-1416-3.
33. Zowe, J., Kočvara, M., Bendsøe, M. P. (1997). Free material optimization via mathematical programming. *Mathematical Programming*, 79(1), 445–466.
34. Xia, Q., Shi, T. (2017). Optimization of composite structures with continuous spatial variation of fiber angle through Shepard interpolation. *Composite Structures*, 182, 273–282. DOI 10.1016/j.compstruct.2017.09.052.
35. Muramatsu, Y., Shimoda, M. (2019). Distributed-parametric optimization approach for free-orientation of laminated shell structures with anisotropic materials. *Structural and Multidisciplinary Optimization*, 59(6), 1915–1934. DOI 10.1007/s00158-018-2163-4.
36. Hao, P., Liu, X., Wang, Y., Liu, D., Wang, B. et al. (2019). Collaborative design of fiber path and shape for complex composite shells based on isogeometric analysis. *Computer Methods in Applied Mechanics and Engineering*, 354, 181–212. DOI 10.1016/j.cma.2019.05.044.
37. Hao, P., Yuan, X., Liu, C., Wang, B., Liu, H. et al. (2018). An integrated framework of exact modeling, isogeometric analysis and optimization for variable-stiffness composite panels. *Computer Methods in Applied Mechanics and Engineering*, 339, 205–238. DOI 10.1016/j.cma.2018.04.046.
38. Hao, P., Yuan, X., Liu, H., Wang, B., Liu, C. et al. (2017). Isogeometric buckling analysis of composite variable-stiffness panels. *Composite Structures*, 165, 192–208. DOI 10.1016/j.compstruct.2017.01.016.
39. Wang, D., Abdalla, M. M., Wang, Z. P., Su, Z. (2019). Streamline stiffener path optimization (SSPO) for embedded stiffener layout design of non-uniform curved grid-stiffened composite (NCGC) structures. *Computer Methods in Applied Mechanics and Engineering*, 344, 1021–1050. DOI 10.1016/j.cma.2018.09.013.
40. Wang, D., Abdalla, M. M., Zhang, W. (2017). Buckling optimization design of curved stiffeners for grid-stiffened composite structures. *Composite Structures*, 159, 656–666. DOI 10.1016/j.compstruct.2016.10.013.
41. Cottrell, A., Hughes, T., Bazilevs, Y. (2009). *Isogeometric analysis: toward integration of CAD and FEA*. London: John Wiley & Sons.
42. Hughes, T. J. R., Cottrell, J. A., Bazilevs, Y. (2005). Isogeometric analysis: CAD, finite elements, NURBS, exact geometry and mesh refinement. *Computer Methods in Applied Mechanics and Engineering*, 194(39), 4135–4195. DOI 10.1016/j.cma.2004.10.008.
43. Bazilevs, Y., Hsu, M. C., Scott, M. A. (2012). Isogeometric fluid-structure interaction analysis with emphasis on non-matching discretizations, and with application to wind turbines. *Computer Methods in Applied Mechanics and Engineering*, 249-252, 28–41. DOI 10.1016/j.cma.2012.03.028.
44. Bazilevs, Y., Takizawa, K., Tezduyar, T. E., Hsu, M. C., Kostov, N. et al. (2014). Aerodynamic and FSI analysis of wind turbines with the ALE-VMS and ST-VMS methods. *Archives of Computational Methods in Engineering*, 21(4), 359–398. DOI 10.1007/s11831-014-9119-7.
45. Benson, D. J., Bazilevs, Y., Hsu, M. C., Hughes, T. J. R. (2011). A large deformation, rotation-free, isogeometric shell. *Computer Methods in Applied Mechanics and Engineering*, 200(13), 1367–1378. DOI 10.1016/j.cma.2010.12.003.
46. Benson, D. J., Hartmann, S., Bazilevs, Y., Hsu, M. C., Hughes, T. J. R. (2013). Blended isogeometric shells. *Computer Methods in Applied Mechanics and Engineering*, 255, 133–146. DOI 10.1016/j.cma.2012.11.020.
47. Hsu, M. C., Bazilevs, Y. (2012). Fluid-structure interaction modeling of wind turbines: simulating the full machine. *Computational Mechanics*, 50(6), 821–833. DOI 10.1007/s00466-012-0772-0.
48. Wall, W. A., Frenzel, M. A., Cyron, C. (2008). Isogeometric structural shape optimization. *Computer Methods in Applied Mechanics and Engineering*, 197(33), 2976–2988. DOI 10.1016/j.cma.2008.01.025.

49. Dedè, L., Borden, M. J., Hughes, T. J. R. (2012). Isogeometric analysis for topology optimization with a phase field model. *Archives of Computational Methods in Engineering*, 19(3), 427–465. DOI 10.1007/s11831-012-9075-z.
50. Kang, P., Youn, S. K. (2016). Isogeometric shape optimization of trimmed shell structures. *Structural and Multidisciplinary Optimization*, 53(4), 825–845. DOI 10.1007/s00158-015-1361-6.
51. Kenway, G. K. W., Martins, J. R. R. A. (2014). Multipoint high-fidelity aerostructural optimization of a transport aircraft configuration. *Journal of Aircraft*, 51(1), 144–160. DOI 10.2514/1.C032150.
52. van Campen, J. M. J. F., Kassapoglou, C., Gürdal, Z. (2012). Generating realistic laminate fiber angle distributions for optimal variable stiffness laminates. *Composites Part B: Engineering*, 43(2), 354–360. DOI 10.1016/j.compositesb.2011.10.014.
53. Locatelli, D., Mulani, S. B., Kapania, R. K. (2011). Wing-box weight optimization using curvilinear spars and ribs (SpaRibs). *Journal of Aircraft*, 48(5), 1671–1684. DOI 10.2514/1.C031336.
54. Hassani, B., Khazadi, M., Tavakkoli, S. M. (2012). An isogeometrical approach to structural topology optimization by optimality criteria. *Structural and Multidisciplinary Optimization*, 45(2), 223–233. DOI 10.1007/s00158-011-0680-5.
55. Lieu, Q. X., Lee, J. (2017). Multiresolution topology optimization using isogeometric analysis. *International Journal for Numerical Methods in Engineering*, 112(13), 2025–2047. DOI 10.1002/nme.5593.
56. Piegl, L., Tiller, W. (1995). *The NURBS Book*. Heidelberg: Springer-Verlag Berlin.
57. Yin, L., Zhang, F., Deng, X., Wu, P., Zeng, H. et al. (2019). Isogeometric bi-directional evolutionary structural optimization. *IEEE Access*, 7, 91134–91145. DOI 10.1109/ACCESS.2019.2927820.
58. de Boor, C. (1972). On calculating with B-splines. *Journal of Approximation Theory*, 6(1), 50–62. DOI 10.1016/0021-9045(72)90080-9.
59. Svanberg, K. (1987). The method of moving asymptotes—a new method for structural optimization. *International Journal for Numerical Methods in Engineering*, 24(2), 359–373. DOI 10.1002/nme.1620240207.
60. Tian, Y., Pu, S., Zong, Z., Shi, T., Xia, Q. (2019). Optimization of variable stiffness laminates with gap-overlap and curvature constraints. *Composite Structures*, 230, 111494. DOI 10.1016/j.compstruct.2019.111494.
61. Blom, A. W., Abdalla, M. M., Gürdal, Z. (2010). Optimization of course locations in fiber-placed panels for general fiber angle distributions. *Composites Science and Technology*, 70(4), 564–570. DOI 10.1016/j.compscitech.2009.12.003.
62. Lindgaard, E., Lund, E. (2011). Optimization formulations for the maximum nonlinear buckling load of composite structures. *Structural and Multidisciplinary Optimization*, 43(5), 631–646. DOI 10.1007/s00158-010-0593-8.
63. Xia, Z., Wang, Y., Wang, Q., Mei, C. (2017). GPU parallel strategy for parameterized LSM-based topology optimization using isogeometric analysis. *Structural and Multidisciplinary Optimization*, 56(2), 413–434. DOI 10.1007/s00158-017-1672-x.